

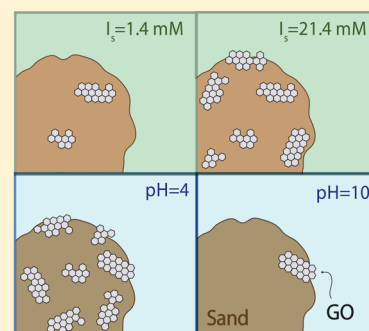
# Interaction Between Graphene Oxide Nanoparticles and Quartz Sand

Nikolaos P. Sotirelis and Constantinos V. Chrysikopoulos\*

School of Environmental Engineering, Technical University of Crete, 73100 Chania, Greece

**S** Supporting Information

**ABSTRACT:** In this study, the influence of pH, ionic strength ( $I_S$ ), and temperature on graphene oxide (GO) nanoparticles attachment onto quartz sand were investigated. Batch experiments were conducted at three controlled temperatures (4, 12, and 25 °C) in solutions with different pH values (pH 4, 7, and 10), and ionic strengths ( $I_S = 1.4, 6.4, \text{ and } 21.4 \text{ mM}$ ), under static and dynamic conditions. The surface properties of GO nanoparticles and quartz sand were evaluated by electrophoretic mobility measurements. Derjaguin–Landau–Verwey–Overbeek (DLVO) potential energy profiles were constructed for the experimental conditions, using measured zeta potentials. The experimental results showed that GO nanoparticles were very stable under the experimental conditions. Both temperature and pH did not play a significant role in the attachment of GO nanoparticles onto quartz sand. In contrast,  $I_S$  was shown to influence attachment. The attachment of GO particles onto quartz sand increased significantly with increasing  $I_S$ . The experimental data were fitted nicely with a Freundlich isotherm, and the attachment kinetics were satisfactorily described with a pseudo-second-order model, which implies that the quartz sand exhibited substantial surface heterogeneity and that GO retention was governed by chemisorption. Furthermore, thermodynamic analysis revealed that the attachment process was nonspontaneous and endothermic, which may be associated with structural changes of the sand surfaces due to chemisorption. Therefore, secondary minimum interaction may not be the dominant mechanism for GO attachment onto the quartz sand under the experimental conditions.



## INTRODUCTION

Graphene was first produced in 2004, and is a single atom-thick sheet of carbon packed in a hexagonal lattice.<sup>1</sup> For this pioneering discovery, Andre K. Geim and Konstantin S. Novoselov, were awarded the Nobel prize in Physics in 2010. This award acknowledged that graphene, owing to its remarkable physicochemical properties (e.g., high specific surface area, high electron mobility, excellent mechanical strength, excellent structural transformability, and high thermal conductivity) is one of the fastest growing nanomaterials that has changed many fields of science, engineering, and industry.<sup>1–4</sup>

Graphene oxide (GO) is a layered nanomaterial that contains graphene sheets and oxygen-bearing functional groups.<sup>5</sup> GO is one of the most important graphene derivatives.<sup>6</sup> Due to its excellent electrochemical properties, GO is used in a wide range of applications. Consequently, the production growth of this material is very rapid, and large quantities of GO particles are expected to eventually reach sensitive environmental systems, including subsurface formations.<sup>7</sup> Note that the solubility of GO in water is very high.<sup>8</sup> Also, the presence of mobile GO particles in surface waters, and groundwater may affect the fate and simultaneous transport (cotransport) of dissolved species and suspended particles (e.g., colloids, biocolloids).<sup>9–11</sup> Furthermore, various studies have reported that GO may be toxic to a variety of mammalian organisms, as well as to human and bacterial cells.<sup>12–17</sup> For this reason, it is important to fully understand the fate of GO in environmental systems, and particularly in groundwater systems, because GO transport in

porous media is significantly affected by the interaction between GO and solid matrix (e.g., sand). Numerous studies published in the literature have focused on the transport of GO in porous media.<sup>18–21</sup> The results of these studies have shown that GO has great colloidal stability and the main factor that affects GO retention in porous media is the ionic strength ( $I_S$ ).

The objective of this work was to improve our understanding of the mechanisms responsible for deposition and attachment of GO nanoparticles onto quartz sand. Batch experiments were conducted, to investigate the effect of temperature, pH, and  $I_S$  on GO attachment onto quartz sand, and GO aggregation, under static and dynamic conditions. The attachment kinetics, related attachment isotherms of GO interactions with quartz sand under different temperatures, and the corresponding thermodynamics were examined. Also, the aggregation of GO and the attachment behavior of GO onto quartz sand were related to theoretically determined DLVO energy interaction profiles. To our knowledge, no previous study has investigated the effect of temperature and pH on GO attachment onto quartz sand.

## MATERIALS AND METHODS

**Graphene Oxide.** High purity SP-1 graphite powder (Bay Carbon Inc., Bay City, MI) was used to produce graphite oxide

Received: July 19, 2015

Revised: October 13, 2015

Accepted: October 14, 2015

Published: October 14, 2015

based on the procedures reported by Hummers et al.<sup>22</sup> The graphite oxide was exfoliated by sonication and centrifugation to obtain graphene oxide flakes.<sup>23</sup> The GO suspensions were prepared by mixing 3 mg of graphene oxide flakes with 250 mL of a phosphate buffered solution (PBS) with low ionic strength ( $I_S = 1.4$  mM). A transmission electron microscopy (TEM) system, JEOL (JEM-2100, operated at 200 kV), equipped with an Erlangshen CCD camera (model 782 ESS00W), was used to record images of GO nanoparticles. The morphology of representative GO flakes is shown in Figure S11. The suspensions with different ionic strengths were adjusted with NaCl; whereas, the suspensions with different pH values were adjusted with either  $H_2PO_4$  or NaOH. Subsequently, the suspensions were sonicated (Elmasonic S 30/(H), Elma Schmidbauer GmbH, Singen, Germany) for 2 h to ensure that the dispersion is thoroughly uniform. It was confirmed that prolonged sonication did not have negative effects (e.g., reaggregation) on GO particles (see Figure S12). All of the solutions were prepared with distilled deionized water ( $ddH_2O$ ). Furthermore, all chemicals employed in this study were of analytical reagent grade, employed without any additional purification.

Calibration curves were prepared, for each set of solution chemistry (pH and  $I_S$ ) examined in this study, in order to establish the relationship between absorbance,  $A_{bs}$  [–], and GO concentration,  $C_{GO}$  [M/L<sup>3</sup>], in the range 0–30 mg/L. A series of diluted samples were prepared from an aqueous solution with known GO concentration, and the absorbance of each diluted sample was measured at the wavelength of  $\lambda_{max} = 231$  nm with a UV–visible spectrophotometer (Cary 400 BIO, Varian, Palo Alto, California). Also, a zetasizer (Nano ZS90, Malvern Instruments, Southborough, MA) was used to measure the zeta potential and hydrodynamic diameter of GO nanoparticles under the various experimental conditions of this study at 25 °C. All zeta potential and hydrodynamic diameter measurements were obtained in triplicates. The sizes of GO nanoparticles under the various experimental conditions of this study are presented in Table S11.

**Sand.** Quartz sand with grain diameter ranging from 0.425 to 0.600 mm (sieve no. 40) was used in this study for the GO attachment experiments. Following the procedures reported by Chrysikopoulos and Aravantinou,<sup>24</sup> the particle-size distribution value determined by sieve analysis was used to calculate the coefficient of uniformity,  $C_u = d_{60}/d_{10} = 1.21$  (where  $d_{10}$ , and  $d_{60}$  is the diameter of a sand grain that is barely too large to pass through a sieve that allows 10%, and 60%, respectively, of the material (by weight) to pass through). The quartz sand employed in this study was relatively uniform because the smaller the value of  $C_u$  the more uniform the sand. Note that  $C_u = 1$  corresponds to uniform sand.<sup>25</sup> The chemical composition of the quartz sand as reported by the manufacturer (Filcom, Netherlands) was: 96.2%  $SiO_2$ , 0.15%  $Na_2O$ , 0.11%  $CaO$ , 0.02%  $MgO$ , 1.75%  $Al_2O_3$ , 0.78%  $K_2O$ , 0.06%  $SO_3$ , 0.46%  $Fe_2O_3$ , 0.03%  $P_2O_5$ , 0.02%  $BaO$ , 0.01%  $Mn_3O_4$ , and 0.28% loss on ignition. The quartz sand was thoroughly cleaned with 0.1 M nitric acid  $HNO_3$  (70%) for 3 h to remove surface impurities (e.g., metal hydroxides and organic coatings), rinsed with distilled deionized water ( $ddH_2O$ ), then soaked in 0.1 M NaOH for 3 h, and rinsed with  $ddH_2O$  again.<sup>26,27</sup> Finally, the quartz sand was dried in an oven at 80 °C. The sand grains were relatively large for direct zeta potential measurement by a zetasizer. Consequently, the sand grains were crushed into fine powder. Several stable suspensions were formed with the

crushed sand, each having a desired ionic strength, which were used for zeta potential measurements.<sup>28,29</sup>

**Batch Experiments.** Both static and dynamic batch experiments were conducted under various solution chemistry conditions at 4, 12, and 25 °C, in order to examine the effect of pH,  $I_S$ , and temperature on GO aggregation and GO attachment on quartz sand. All batch experiments were performed in 20 mL Pyrex glass screw-cap tubes (Fisher Scientific). Glass tubes were washed with detergent, rinsed thoroughly in  $ddH_2O$ , autoclave sterilized, and oven-dried at 80 °C overnight. A PBS solution with  $I_S = 1.35$  mM was prepared with 0.001 M phosphate buffer salts in  $ddH_2O$  and adjusted to a pH 7.2 with NaOH. The PBS solution was used to stabilize the pH of GO dispersion.<sup>5</sup> Note that the relatively wide temperature range (4–25 °C), and pH range (4–10) considered in this study is representative of the conditions observed in various ground and surface waters.<sup>30</sup>

For each experiment, 16 glass tubes were employed, which were divided into two groups. Each group consisted of eight glass tubes. The glass tubes of the first group (experimental tubes) contained 14 mL of GO dispersion with 14 g of sand, and the glass tubes of the second group (control tubes) contained 20 mL of GO dispersion without sand. All glass tubes were filled to the top. However, a small air bubble was always trapped within the tubes when the caps were screwed onto the tubes. Both groups were treated in the same manner. The experiments at 4 and 12 °C were conducted in an incubator (Foc 120E, Velp Scientifica, Italy). The dynamic batch experiments were performed with the tubes attached to a rotator (Selecta, Agitador orbit), operated at 12 rpm, in order to allow the sand to mix within the GO suspension. Control tubes, in the absence of sand, were used to monitor GO aggregation and possible GO attachment onto the walls of the glass tubes. A sample of the PBS solution (3.0 mL) was removed from each selected glass tube at different preselected times (0, 5, 10, 20, 30, 60, 90, 120, 180, 240 min) and the GO concentration was measured in triplicates. All used glass tubes were discarded. The experimental conditions of the various batch experiments conducted in this study are summarized in Table S12.

## THEORETICAL ANALYSIS OF GO-SAND INTERACTIONS

Assuming that GO particles are practically colloids, the classical theory developed by Derjaguin–Landau–Verwey–Overbeek (DLVO) is applicable. Based on the DLVO theory, the total interaction energy between two surfaces (here GO and quartz sand) equals the arithmetic sum of the van der Waals  $\Phi_{vdW}$ , double layer,  $\Phi_{dl}$ , and Born,  $\Phi_{Born}$  potential energies:<sup>26</sup>

$$\Phi_{DLVO}(h) = \Phi_{vdW}(h) + \Phi_{dl}(h) + \Phi_{Born}(h) \quad (1)$$

where  $h$  [m] is the separation distance between the approaching surfaces.

Following the work by Chrysikopoulos and Syngouna,<sup>31</sup> for the case of two approaching surfaces, the  $\Phi_{vdW}$  [J] interactions were calculated with the expression provided by Gregory,<sup>32</sup> using  $\lambda \approx 10^{-7}$  m for the characteristic wavelength of the sphere-plate or plate-plate interactions, and  $A_{123} = 6.26 \times 10^{-21}$  [J] for the combined Hamaker constant for the system GO-water-quartz sand.<sup>18,19</sup> The  $\Phi_{dl}$  for sphere-plate interactions were calculated with the expression provided by Hogg et al.,<sup>33</sup> using  $N_A = 6.02 \times 10^{23}$  [1/mol] for the Avogadro's number,  $e = 1.602 \times 10^{-19}$  [C] for the elementary charge, and

$k_B = 1.38 \times 10^{-23}$  [J/K] for the Boltzmann constant. The  $\Phi_{\text{Born}}$  [J] for sphere-plate was estimated by the relationship provided by Ruckenstein et al.<sup>34</sup> Note that  $\Phi_{\text{Born}}$  can easily be neglected if  $h > 1$  nm. The effect of Born interaction may not be of great significance in aqueous systems due to the possible presence of hydrated ions, which prevent surface-surface separation distances to approach  $h \sim 0.3$  nm.<sup>31</sup>

For the case of two approaching surfaces, both with planar geometries (plate-plate), the  $\Phi_{\text{vdW}}$  [J],  $\Phi_{\text{dl}}$  [J], and  $\Phi_{\text{Born}}$  [J] interactions were calculated with the equations provided by Gregory,<sup>32</sup> Hogg et al.,<sup>33</sup> and Mahmood et al.,<sup>35</sup> respectively. All the details associated with the DLVO calculations are presented in the Supporting Information section.

## RESULTS AND DISCUSSION

**Zeta Potentials and DLVO Interactions.** Figure S13 illustrates graphically the measured zeta potential values of GO and quartz sand at various pH values. Both GO and quartz sand are negatively charged for all the pH values examined in this study ( $2 \leq \text{pH} \leq 10$ ), suggesting that GO-sand and GO-GO interactions are repulsive. Similar findings for GO-sand and GO-GO interactions have been reported in the literature by several other investigators.<sup>18–20</sup> Zeta potential values can also be used to evaluate the stability of suspended particles. Note that the zeta potentials of both GO and quartz sand decrease with increasing pH, suggesting that the suspended particles become more stable with increasing pH. It is worthy to note that the stability of suspended particles is expected to increase with increasing absolute zeta potential values.<sup>36</sup> At relatively low absolute zeta potential values aggregates may form, because existing attractive forces may be stronger than the repulsive forces.<sup>37</sup> The commonly used threshold for absolute zeta potential value for stable colloidal suspensions is considered to be  $>30$  mV.<sup>38,39</sup> Therefore, based on the data of Figure S13 and preliminary laboratory observations, particle suspensions with  $\text{pH} < 4$  are not desired, because both GO and quartz sand are not stable. It was confirmed that no aggregation of GO nanoparticles in suspension occurred for the duration of the experiments (see Figure S14).

The absolute zeta potential value of both the GO and quartz sand suspensions decreased, or equivalently the zeta potential values became less negative, with increasing  $I_s$ , due to suppression of the electric double layer.<sup>18,19,36</sup> However, the zeta potential values were consistently greater for GO than quartz sand particles. The measured zeta potential values of GO and quartz sand for three  $I_s$  values (1.4, 6.4, 21.4 mM) are illustrated graphically in Figure S15.

DLVO interaction energy profiles are characterized by a deep energy “well”, which appears at relatively small separation distances and it is known as the primary minimum,  $\Phi_{\text{min}1}$ , the energy barrier to attachment and detachment known as the primary maximum,  $\Phi_{\text{max}1}$ , and a shallow energy “well” at relatively large separation distances known as the secondary minimum,  $\Phi_{\text{min}2}$ .<sup>31,40</sup> In this work, the sphere-plate approximation was employed for the estimation of GO-sand interactions, because the GO particles are so much smaller than the quartz sand, and plate-plate for GO-GO interactions. Certainly, GO particles (flakes) are not perfect spheres. However, for GO particles in the vicinity of quartz sand, it is reasonable to assume that GO particles are more sphere-like and sand particles more plate-like. Note that calculations of interaction forces between GO particles and quartz sand have been presented in the literature using either the sphere-plate

approximation,<sup>19,41</sup> or the plate-plate approximation.<sup>21,42</sup> Also, the interaction forces were intentionally calculated for  $h > 0.3$  nm, rendering the effect of Born interaction as insignificant. Consequently, the interaction energy profiles constructed do not exhibit a  $\Phi_{\text{min}1}$ .

The simulated GO-sand (sphere-plate) interactions energy profiles (see Figures 1a,b) exhibit a shallow  $\Phi_{\text{min}2}$ , and a very

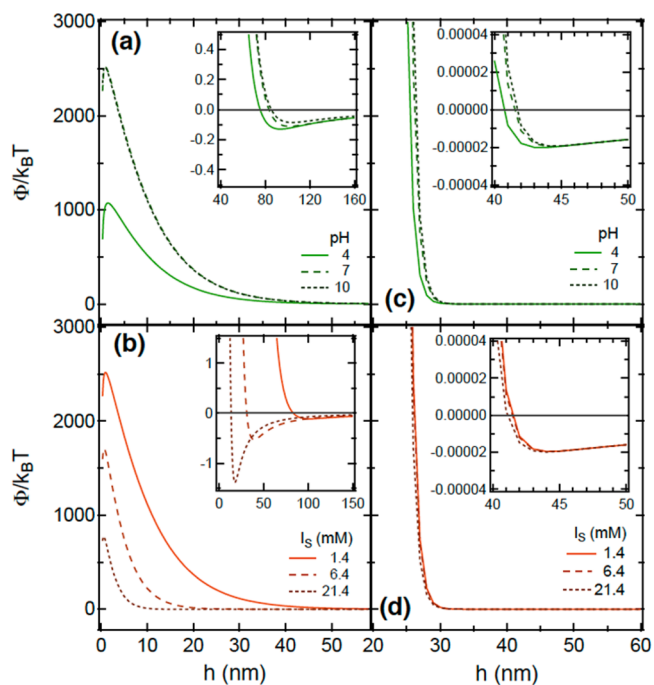


**Figure 1.** Calculated DLVO total interaction energy profiles between GO and sand (a, b), and between GO and GO (c, d), as a function of separation distance for the experimental conditions. Each figure-insert highlights the corresponding secondary energy minima.

high  $\Phi_{\text{max}1}$ . Note that the lowest  $\Phi_{\text{max}1}$  and deepest  $\Phi_{\text{min}2}$  were observed for pH 4 (see Figure 1a). Note that,  $\Phi_{\text{max}1}$  was smallest for the highest  $I_s$  examined in this study (see Figure 1b), similar trend has been observed by other investigators.<sup>19</sup> Also, as expected,  $\Phi_{\text{min}2}$  was deepest for the highest  $I_s$ . Furthermore, the simulated GO-GO (plate-plate) interaction energy profiles (see Figures 1c,d) suggest that there is a very shallow  $\Phi_{\text{min}2}$ , and very high  $\Phi_{\text{max}1}$ , suggesting the presence of strong repulsive forces between GO nanoparticles. Clearly, fluctuations in both pH and  $I_s$  do not play a significant role in the GO-GO interactions energy profiles. This is in agreement with previous findings that for typical environmental systems (pH 5–9), GO aggregation is not significantly affected by pH.<sup>19</sup> It is worthy to note that  $\Phi_{\text{min}2}$  is very shallow for all cases examined here (see Figure 1). Therefore, secondary minimum interaction is an unlike mechanism for GO attachment onto the quartz sand and GO aggregation. However, DLVO interaction energy profiles do not account for surface roughness, angularity, chemical impurities, and surface charge heterogeneity of the sand, which are known to produce local areas of favorable interaction that lead to attachment even under unfavorable conditions.<sup>43–45</sup> Although in this study the quartz sand was thoroughly cleaned to eliminate surface charge heterogeneity, charge heterogeneities from the sand surfaces cannot be ruled out.<sup>46,47</sup>

**Isotherm Batch Experiments.** The experimental data from the GO equilibrium attachment onto quartz sand at three different temperatures where fitted nicely with a Freundlich isotherm (the linear and Langmuir isotherm models were also tested, see Table S13), which has been employed in various contaminant, colloid and biocolloid attachment studies of environmental significance.<sup>24,31,48,49</sup> The Freundlich isotherm is a nonlinear relationship between the aqueous phase GO concentration at equilibrium,  $C_{eq}$  [ $M_n/L^3$ ], in units of [mg GO/Liter of solution], and the GO concentration adsorbed onto the quartz sand at equilibrium,  $C_{eq}^*$  [ $M_n/M_s$ ], in units of [mg GO/g sand]:<sup>50</sup>

$$C_{eq}^* = K_f C_{eq}^m \quad (2)$$

where  $K_f$  [ $L^{3+m}/M_s M_n^{m-1}$ ] is the Freundlich constant in units of [(liter of solution)<sup>m</sup>/(g sand) (mg GO)<sup>m-1</sup>],  $m$  [-] is the Freundlich exponent, which is equal to one for linear deposition and attachment. Also, for notational convenience  $M_n$  was introduced for the mass of nanoparticles (GO), and  $M_s$  for the mass of solids (quartz sand). Note that the Freundlich isotherm describes equilibrium attachment onto heterogeneous sorbent surfaces, and contrary to Langmuir isotherm, does not assume monolayer deposition.<sup>24</sup> The Freundlich parameter  $m$  is a measure of the surface heterogeneity of the quartz sand (the smaller the value of  $m$  the higher the surface heterogeneity of the quartz sand), and  $K_f$  is directly proportional to the deposition and attachment capacity of the quartz sand. For the estimation of the Freundlich parameters the linearized form of the Freundlich isotherm was used:

$$\log C_{eq}^* = \log K_f + m \log C_{eq} \quad (3)$$

The parameters  $m$  and  $\log K_f$  were estimated by the slope and ordinate (vertical axis intercept), respectively, of the linear plot of the experimental data in the form of  $\log C_{eq}^*$  versus  $\log C_{eq}$ . The static and dynamic attachment data for the experiments conducted in this study at three different temperatures are presented in Figure 2, and the corresponding Freundlich isotherm parameters are listed in Table 1. The model fittings of the experimental data were obtained with the graphical statistical software "IGOR-Pro" (WaveMetrics Inc.).

Based on the calculated  $R^2$  values (see Figure 2 and Table 1), the Freundlich isotherm model fits very well the experimental data under static as well as dynamic conditions. The number of accessible attachment sites is much higher in dynamic than static experiments due to agitation, which improves the contact of quartz sand grains with the liquid and decreases the resistance to mass transfer.<sup>51-53</sup> Therefore, more GO particles were adsorbed onto the quartz sand under dynamic than static conditions (compare the  $K_f$  values listed in Table 1). This finding is in agreement with other attachment studies.<sup>24,31</sup> The attachment of GO nanoparticles onto quartz sand was a favorable process because all of the estimated  $m$  values were less than unity ( $m < 1$ ). Also, the  $K_f$  values listed in Table 1 suggest that for most of the cases examined in this study the attachment of GO nanoparticles increases with increasing temperature.

**Kinetic Batch Experiments.** The experimental data from the kinetic batch attachment experiments were fitted with the following pseudo-second-order expression:<sup>48,54</sup>

$$\frac{dC_t^*}{dt} = k_{p2}(C_{eq}^* - C_t^*)^2 \quad (4)$$

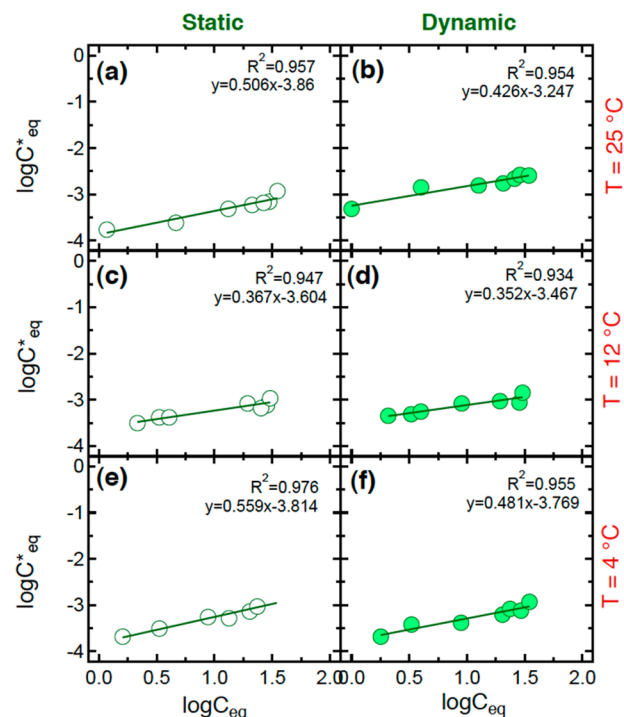


**Figure 2.** Linearized Freundlich isotherms for GO nanoparticles attachment onto quartz sand at three different temperatures: (a, b) 25 °C, (c, d) 12 °C, and (e, f) 4 °C. The open circles indicate static conditions and the solid circles dynamic conditions. The solid lines are the linear regressions with slope equal to  $m$ , and ordinate equal to  $\log K_f$  (Here pH 7 and  $I_s = 1.4$  mM).

**Table 1.** Freundlich Parameters for GO Equilibrium Attachment onto Quartz Sand for pH 7 and  $I_s = 1.4$  mM

$T$ (°C)	$m$ (-)	$K_f$ [ $L^{3+m}/(g \text{ sand}) (mg \text{ GO})^{m-1}$ ]	$R^2$
Static			
4	0.56	1.54	0.976
12	0.37	2.49	0.947
25	0.51	1.37	0.957
Dynamic			
4	0.48	1.70	0.955
12	0.35	3.41	0.934
25	0.43	5.02	0.954

where  $t$  [ $t$ ] is time;  $C_t^*$  [ $M_n/M_s$ ] is the GO concentration adsorbed onto quartz sand at time  $t$ ; and  $k_{p2}$  [ $M_s/(M_n \cdot t)$ ] is the rate constant of the pseudo-second order attachment. Separating variables and integrating the time variable from 0 to  $t$ , and the GO concentration adsorbed onto quartz sand from 0 to  $C_t^*$  yields

$$C_t^* = \frac{(C_{eq}^*)^2 k_{p2} t}{1 + C_{eq}^* k_{p2} t} \quad (5)$$

The above expression can easily be rearranged in a linear form (see Supporting Information). A pseudo-second-order kinetic model indicates that for a liquid–solid system, removal from liquid (aqueous) phase is governed by physicochemical interactions (chemisorption).<sup>54,55</sup> Note that pseudo-second-order models were applied initially in soil science to describe reactions between minerals and soil.<sup>56</sup> This kinetic model has been used successfully to describe the kinetics of *Bacillus subtilis*

attachment onto single-walled carbon nanotubes,<sup>57</sup> as well as the kinetics of *P. putida* attachment onto kaolinite.<sup>9</sup>

The various kinetic attachment experimental data were fitted with eq 5, and the results are presented in Figures 3–5,

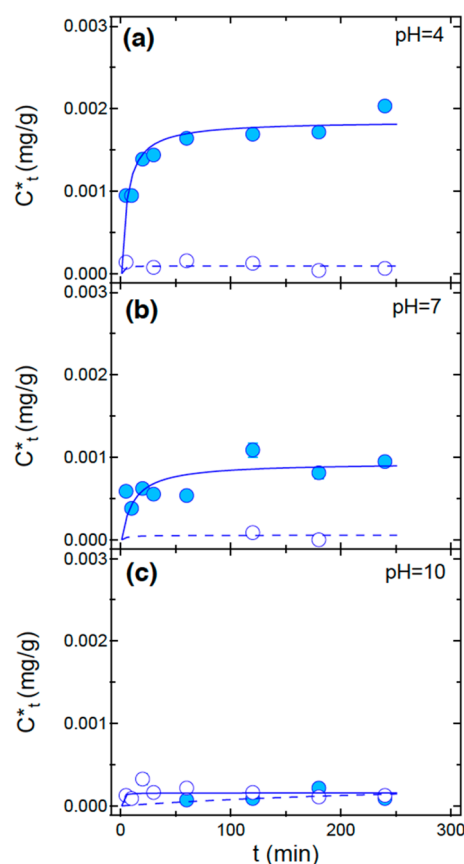


**Figure 3.** Effect of pH on GO kinetic attachment onto quartz sand. The symbols (circles) represent the experimental data, and the curves the fitted model simulations. The open and solid circles correspond to static and dynamic conditions, respectively. Also, the dashed and solid curves correspond to the fitted model simulations under static and dynamic conditions, respectively. Error bars are not shown, because they are smaller than the symbols. Here,  $I_s = 1.4$  mM and  $T = 25$  °C.

respectively. The fitted kinetic model-parameter-values for  $k_{p2}$  and  $C_{eq}^*$  are listed in Table 2. The pseudo-second-order model was fitted to the experimental data with the in-house developed nonlinear least-squares regression software “ColloidFit,” which incorporates the state of the art model-independent parameter estimation package “Pest”.<sup>58</sup> Furthermore, the amount of the GO nanoparticles attached onto the quartz sand, in the various kinetic batch experiments conducted for this work, are listed in Table S14.

Clearly, Figures 3–5 show that more GO mass is adsorbed onto quartz sand under dynamic than static conditions. Actually, GO attachment under static conditions is negligible. This is an intuitive result, attributable to agitation, and in perfect agreement with the isotherm batch experimental results of this study. Also, worthy to note is that, for all cases examined in this study, GO attachment onto quartz sand was relatively fast, reaching equilibrium within 70–100 min (see Figures 3–5).

Figure 3 shows the influence of pH on GO attachment onto quartz sand. The observed increase in GO nanoparticle mass

**Table 2.** Fitted Parameters Obtained From the GO Kinetic Attachment Experiments

Experimental Conditions				
pH	$I_s$ (mM)	T (°C)	$C_{eq}^*$ [mg GO/g sand]	$k_{p2}$ [g sand/(mg GO-min)]
Static				
4	1.4	25	0.0018	212.0
7	1.4	25	0.0010	42.9
10	1.4	25	0.0010	560
7	6.4	25	0.0011	19.9
7	21.4	25	0.0012	206.6
7	1.4	4	0.0008	91.9
7	1.4	12	0.0009	171.3
Dynamic				
4	1.4	25	0.0029	89.2
7	1.4	25	0.0014	97.8
10	1.4	25	0.0014	92.1
7	6.4	25	0.0023	166.8
7	21.4	25	0.0044	49.9
7	1.4	4	0.0012	69.2
7	1.4	12	0.0014	365.4

adsorbed onto the quartz sand with decreasing pH values is attributed to the decreasing absolute zeta potential values with decreasing pH (see Figure S13), and to deeper  $\Phi_{min2}$ , as predicted by the DLVO theory (see Figure 1a).

Figure 4 shows that increasing  $I_s$  leads to a significant increase in GO attachment onto the quartz sand. Note that increasing  $I_s$  leads to smaller absolute zeta potential values (see Figure S15), and to deeper  $\Phi_{min2}$ , as predicted by the DLVO theory (see Figure 1b). This finding is in agreement with results reported by other investigators.<sup>18–20</sup>

Figure 5 shows the influence of temperature on GO attachment onto quartz sand. Clearly, the experimental data suggest that temperature does not play significant role in GO attachment onto quartz sand. However, as expected, there is a slight increase in attachment rate with increasing temperature.

**Attachment Thermodynamics.** The thermodynamic behavior of GO nanoparticle attachment onto quartz sand was investigated from the temperature dependent attachment isotherms by estimating the standard Gibbs free energy change,  $\Delta G^\circ$  [kJ/mol], the standard enthalpy change,  $\Delta H^\circ$  [kJ/mol], and the standard entropy change,  $\Delta S^\circ$  [J/mol·K], which can determine whether the attachment process is spontaneous, and endothermic or exothermic. The  $\Delta G^\circ$  at a selected temperature can be obtained from the following thermodynamic relationship:

$$\Delta G^\circ = -R_a T \ln K_0 \quad (6)$$

where  $R_a = 8.3145$  [J/(mol·K)] is the universal gas constant, and  $T$  [K] is the absolute temperature, and  $K_0$  [ $L^3/M$ ] is the thermodynamic attachment equilibrium constant, also known as the thermodynamic distribution coefficient, which can be obtained from the intercept with the vertical axis of the linear plot of  $\ln[C_{eq}^*/C_{eq}]$  versus  $C_{eq}^*$ .<sup>59,60</sup> Furthermore, the values of  $\Delta H^\circ$  and  $\Delta S^\circ$  can be obtained from the following thermodynamic relationship:

$$\ln K_0 = \frac{\Delta S^\circ}{R_a} - \frac{\Delta H^\circ}{R_a T} \quad (7)$$

Note that the slope and ordinate (vertical axis intercept) of a linear plot of  $\ln K_0$  versus  $1/T$  correspond to the  $\Delta H^\circ/R_a$  and

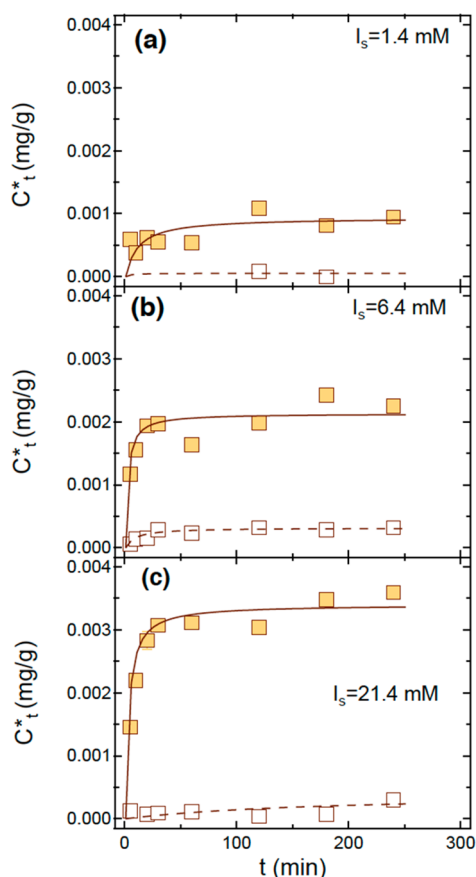


**Figure 4.** Effect of ionic strength on GO kinetic attachment onto quartz sand. The symbols (squares) represent the experimental data, and the curves the fitted model simulations. The open and solid squares correspond to static and dynamic conditions, respectively. Also, the dashed and solid curves correspond to the fitted model simulations under static and dynamic conditions, respectively. Error bars are not shown, because they are smaller than the symbols. Here, pH 7 and  $T = 25\text{ }^{\circ}\text{C}$ .

$\Delta S^{\circ}/R_a$ , respectively. The values of  $K_0$ , for both static and dynamic experiments are estimated from the experimental data presented in Figure 6; whereas,  $\Delta G^{\circ}$ ,  $\Delta H^{\circ}$ , and  $\Delta S^{\circ}$  are obtained from the linear plots presented in Figure 7. All linear regressions were obtained with the graphical statistical software “IGOR-Pro” (WaveMetrics Inc.). The resulting thermodynamic parameter values are listed in Table 3. Note that the value of  $K_0$  increased with temperature suggesting that the attachment process was endothermic. The positive values of  $\Delta G^{\circ}$  indicated that the attachment process was nonspontaneous. Also, the positive values of  $\Delta H^{\circ}$  indicated that the attachment process was endothermic. Finally, the value of  $\Delta S^{\circ}$  for static experiments was negative indicating that the attachment process was enthalpy driven, whereas for the dynamic experiments was positive indicating high affinity of the quartz sand for GO nanoparticles, and increased randomness at the solid/liquid interface.<sup>61</sup> The observed nonspontaneity and endothermic nature of the attachment process is associated with structural changes of the sand surfaces due to chemisorption.

### ENVIRONMENTAL IMPLICATION

The results of this study have shown that GO nanoparticle retention by quartz sand can be described by the Freundlich

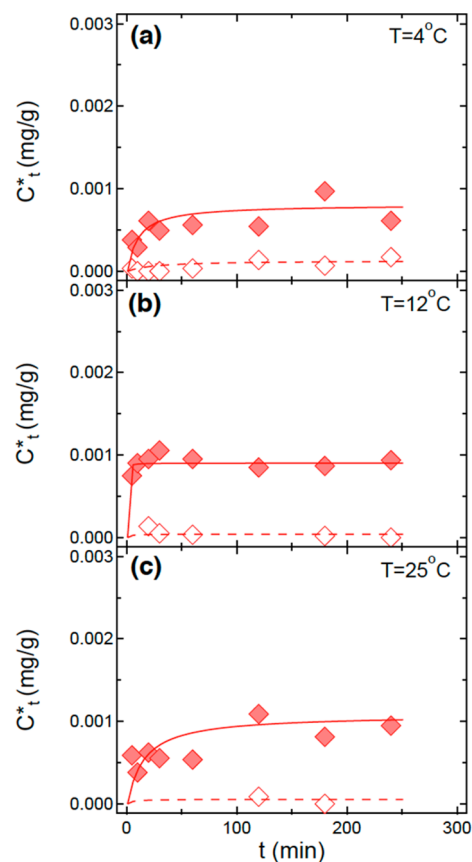


**Figure 5.** Effect of temperature on GO kinetic attachment onto quartz sand. The symbols (diamonds) represent the experimental data, and the curves the fitted model simulations. The open and solid diamonds correspond to static and dynamic conditions, respectively. Also, the dashed and solid curves correspond to the fitted model simulations under static and dynamic conditions, respectively. Error bars are not shown, because they are smaller than the symbols. Here, pH 7 and  $I_s = 1.4\text{ mM}$ .

isotherm and pseudo-second-order kinetics, suggesting that the quartz sand exhibited surface heterogeneities. Thermodynamic analysis revealed that the GO attachment process was endothermic and nonspontaneous, which is consistent with chemisorption. It was demonstrated that temperature did not significantly affect GO attachment onto quartz sand. Also, GO attachment increased considerably only for high  $I_s$  and low pH values. Finally, it was observed that fluctuations in both pH and  $I_s$  may not play a significant role in the GO aggregation. The amount of GO particles retained by deposition and attachment was very small ( $\sim 0.2\text{ }\mu\text{g/g}$  static, and  $\sim 1.4\text{ }\mu\text{g/g}$  dynamic). This observation is in agreement with values reported by other investigators.<sup>18</sup> Furthermore, these results suggested that GO particle capture may not be attributed to secondary minimum deposition, but to chemical interactions between the GO particles and the sand surfaces. Although GO aggregation is not important under the experimental conditions of this study (pH 4–10,  $I_s = 1.4\text{--}21.4\text{ mM}$ , and  $T = 4\text{--}25\text{ }^{\circ}\text{C}$ ), this will not be the case in water saturated subsurface formations where metal cations are present. Note that Wu et al.<sup>42</sup> observed significant GO aggregation in the presence of divalent metal ions. Also, Sun et al.<sup>21</sup> reported that the size of GO particles increased with travel distance during transport in columns packed with sand. Furthermore, in subsurface environments where the solid matrix incorporates a variety of rough surfaces with a wide

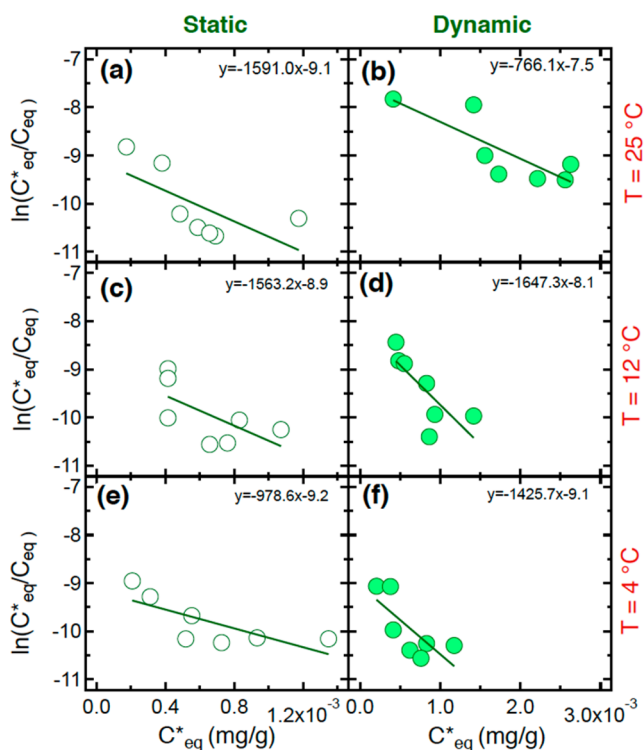


**Figure 6.** Linear plots of  $\ln[C_{eq}^*/C_{eq}]$  versus  $C_{eq}^*$  at three different temperatures: (a, b) 25 °C, (c, d) 12 °C, and (e, f) 4 °C. The open circles indicate static conditions and the solid circles dynamic conditions.

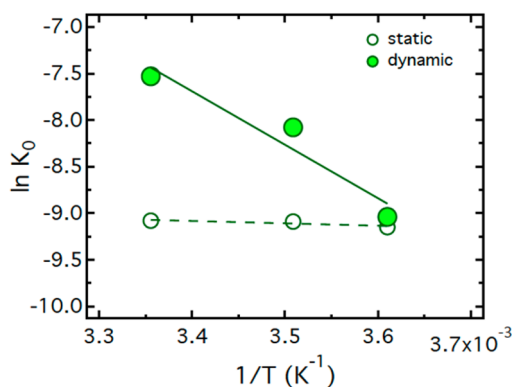


**Figure 7.** Linear plot of  $\ln K_0$  versus  $1/T$ .

**Table 3. Values of Thermodynamic Parameters for GO Attachment onto Quartz Sand**

T (°C)	$K_0$ (L/g)	$\Delta G^\circ$ (kJ/mol)	$\Delta H^\circ$ (kJ/mol)	$\Delta S^\circ$ (J/mol·K)
Static				
4	$1.06 \times 10^{-4}$	21.1	1.9	-69.1
12	$1.12 \times 10^{-4}$	21.6		
25	$1.13 \times 10^{-4}$	22.5		
Dynamic				
4	$1.19 \times 10^{-4}$	20.8	47.8	98.5
12	$3.10 \times 10^{-4}$	19.1		
25	$5.37 \times 10^{-4}$	18.7		

range of charge heterogeneities and reactive minerals, enhanced GO deposition and attachment is expected to crucially impact GO fate and transport.

## ■ ASSOCIATED CONTENT

### Supporting Information

The Supporting Information is available free of charge on the ACS Publications website at DOI: 10.1021/acs.est.5b03496.

Details of DLVO theory, additional mathematical expressions of the pseudo-second-order kinetic model, transmission electron micrograph images of GO flakes, the effect of solution pH on the zeta potential of GO and quartz sand suspensions, the effect of ionic strength on the zeta potential of GO and quartz sand, the effect of sonication time on the size of GO aggregates, the effect of time on the size of GO aggregates, the GO aggregate size under different experimental conditions, a compilation of kinetic batch experimental conditions, comparison of the  $R^2$  values of the three isotherm models tested, and the amount of GO attached onto quartz sand in the various kinetic batch experiments can be found in the Supporting Information section (PDF)

## ■ AUTHOR INFORMATION

### Corresponding Author

\*Fax: +30 28210 37847; e-mail: [cvc@enveng.tuc.gr](mailto:cvc@enveng.tuc.gr).

### Notes

The authors declare no competing financial interest.

## ■ ACKNOWLEDGMENTS

This research has been cofinanced by the European Union (European Social Fund-ESF) and Greek national funds through the Operational program “Education and Lifelong Learning” under the action Aristeia I (Code1185). We are thankful to N. Xekoukoulotakis for valuable laboratory assistance, and to D. Theodoridis for recording the TEM images.

## ■ REFERENCES

- Geim, A. K. Graphene: Status and prospects. *Science* **2009**, *324* (5934), 1530–1534.
- Novoselov, K. S.; Geim, A. K.; Morozov, S. V.; Jiang, D.; Zhang, Y.; Dubonos, S. V.; Grigorieva, I. V.; Firsov, A. A. Electric field effect in atomically thin carbon films. *Science* **2004**, *306* (5696), 666–669.
- Green, A. A.; Hersam, M. C. Solution phase production of graphene with controlled thickness via density differentiation. *Nano Lett.* **2009**, *9* (12), 4031–4036.
- Duch, M. C.; Budinger, G. R. S.; Liang, Y. T.; Soberanes, S.; Ulrich, D.; Chiarella, S. E.; Campochiaro, L. A.; Gonzalez, A.; Chandel, N. S.; Hersam, M. C.; Mutlu, G. M. Minimization of oxidation and stable nanoscale dispersion improves the biocompatibility of graphene in the lung. *Nano Lett.* **2011**, *11* (12), 5201–5207.
- Dreyer, D. R.; Park, S.; Bielawski, C. W.; Ruoff, R. S. The chemistry of graphene oxide. *Chem. Soc. Rev.* **2010**, *39*, 228–240.
- Chen, D.; Feng, H.; Li, J. Graphene Oxide: Preparation, Functionalization, and Electrochemical Applications. *Chem. Rev.* **2012**, *112* (11), 6027–6053.
- Salas, E. C.; Sun, Z.; Lutge, A.; Tour, J. M. Reduction of graphene oxide via bacterial respiration. *ACS Nano* **2010**, *4*, 4852–4856.
- Mkhoyan, K. A.; Contryman, A. W.; Silcox, J.; Stewart, D. A.; Eda, G.; Mattevi, C.; Miller, S.; Chhowalla, M. Atomic and electronic structure of graphene-oxide. *Nano Lett.* **2009**, *9* (3), 1058–1063.
- Vasiliadou, I. A.; Chrysikopoulos, C. V. Cotransport of *Pseudomonas putida* and kaolinite particles through water saturated columns packed with glass beads. *Water Resour. Res.* **2011**, *47* (2), W02543.

- (10) Syngouna, V. I.; Chrysikopoulos, C. V. Cotransport of clay colloids and viruses in water saturated porous media. *Colloids Surf, A* **2013**, *416*, 56–65.
- (11) Syngouna, V. I.; Chrysikopoulos, C. V. Experimental investigation of virus and clay particles cotransport in partially saturated columns packed with glass beads. *J. Colloid Interface Sci.* **2015**, *440*, 140–150.
- (12) Akhavan, O.; Ghaderi, E. Toxicity of graphene and graphene oxide nanowalls against bacteria. *ACS Nano* **2010**, *4* (10), 5731–5736.
- (13) Wang, K.; et al. Biocompatibility of graphene oxide. *Nanoscale Res. Lett.* **2011**, *6* (1), 1–8.
- (14) Chang, Y.; Yang, S. T.; Liu, J. H.; Dong, E.; Wang, Y.; Cao, A.; Liu, Y.; Wang, H. In vitro toxicity evaluation of graphene oxide on A549 cells. *Toxicol. Lett.* **2011**, *200* (3), 201–210.
- (15) Vallabani, N. V. S.; Mittal, S.; Shukla, R. K.; Pandey, A. K.; Dhakate, S. R.; Pasricha, R.; Dhawan, A. Toxicity of graphene in normal human lung cells (BEAS-2B). *J. Biomed. Nanotechnol.* **2011**, *7* (1), 106–107.
- (16) Singh, S. K.; Nayak, M. K.; Kumari, S.; Gracio, J. J. A.; Dash, D. Characterization of graphene oxide by flow cytometry and assessment of its cellular toxicity. *J. Biomed. Nanotechnol.* **2011**, *7* (1), 30–31.
- (17) Hu, C.; Wang, Q.; Zhao, H.; Wang, L.; Guo, S.; Li, X. Ecotoxicological effects of graphene oxide on protozoan *Euglena gracilis*. *Chemosphere* **2015**, *128*, 184–190.
- (18) Feriencikova, L.; Xu, S. Deposition and remobilization of graphene oxide within saturated sand packs. *J. Hazard. Mater.* **2012**, *235–236*, 194–200.
- (19) Lanphere, J. D.; Luth, C. J.; Walker, S. L. Effects of Solution Chemistry on the Transport of Graphene Oxide in Saturated Porous Media. *Environ. Sci. Technol.* **2013**, *47*, 4255–4261.
- (20) Liu, L.; Gao, B.; Wu, L.; Morales, V. L.; Yang, L.; Zhou, Z.; Wang, H. Deposition and transport of graphene oxide in saturated and unsaturated porous media. *Chem. Eng. J.* **2013**, *229*, 444–449.
- (21) Sun, Y.; Gao, B.; Bradford, S. A.; Wu, L.; Chen, H. Transport, retention, and size perturbation of graphene oxide in saturated porous media: Effects of input concentration and grain size. *Water Res.* **2015**, *68*, 24–33.
- (22) Hummers, W. S.; Offeman, R. E. Preparation of Graphitic Oxide. *J. Am. Chem. Soc.* **1958**, *80* (6), 1339–1339.
- (23) Zhang, T.-Y.; Zhang, D. Aqueous colloids of graphene oxide nanosheets by exfoliation of graphite oxide without ultrasonication. *Bull. Mater. Sci.* **2011**, *34* (1), 25–28.
- (24) Chrysikopoulos, C. V.; Aravantinou, A. F. Virus attachment onto quartz sand: Role of grain size and temperature. *J. Environ. Chem. Eng.* **2014**, *2*, 796–801.
- (25) Holtz, R. D.; Kovacs, W. D. *An Introduction to Geotechnical Engineering*; Prentice Hall: New Jersey, 1981.
- (26) Loveland, J. P.; Ryan, J. N.; Amy, G. L.; Harvey, R. W. The reversibility of virus attachment to mineral surfaces. *Colloids Surf, A* **1996**, *107*, 205–221.
- (27) Xu, S. P.; Liao, Q.; Sayers, J. E. Straining of nonspherical colloids in saturated porous media. *Environ. Sci. Technol.* **2008**, *42*, 771–778.
- (28) Stephan, E. A.; Chase, G. G. A preliminary examination of zeta potential and deep bed filtration activity. *Sep. Purif. Technol.* **2001**, *21*, 219–226.
- (29) Mitropoulou, P. N.; Syngouna, V. I.; Chrysikopoulos, C. V. Transport of colloids in unsaturated packed columns: Role of ionic strength and sand grain size. *Chem. Eng. J.* **2013**, *232*, 237–248.
- (30) Collins, W. D. *Temperature of Water Available for Industrial Use in the United States*; Department of the Interior, U.S. Geological Survey, Water Supply Paper 520-F, 1925.
- (31) Chrysikopoulos, C. V.; Syngouna, V. I. Attachment of bacteriophages MS2 and  $\Phi$ X174 onto kaolinite and montmorillonite: Extended-DLVO interactions. *Colloids Surf, B* **2012**, *92*, 74–83.
- (32) Gregory, J. Approximate expressions for retarded van der Waals interaction. *J. Colloid Interface Sci.* **1981**, *83* (1), 138–145.
- (33) Hogg, R.; Healy, T. W.; Fuersten, D. W. Mutual coagulation of colloidal dispersions. *Trans. Faraday Soc.* **1966**, *62*, 1638–1651.
- (34) Ruckenstein, E.; Prieve, D. C. Adsorption and Desorption of Particles and Their Chromatographic Separation. *AIChE J.* **1976**, *22*, 276.
- (35) Mahmood, T.; Amiratharajah, A.; Sturm, T. W.; Dennett, K. E. A micromechanics approach for attachment and detachment of symmetric colloidal particles. *Colloids Surf, A* **2001**, *177*, 99–110.
- (36) Sygouni, V.; Chrysikopoulos, C. V. Characterization of TiO<sub>2</sub> nanoparticle suspensions in aqueous solutions and TiO<sub>2</sub> nanoparticle retention in water-saturated columns packed with glass beads. *Chem. Eng. J.* **2015**, *262*, 823–830.
- (37) Elimelech, M.; Gregory, J.; Jia, X.; Williams, R. A. *Particle Deposition and Aggregation: Measurement, Modeling and Simulation*; Butterworth Heinemann: Oxford, U.K., 1995.
- (38) Riddick, E. M. *Control of Colloid Stability through Zeta Potential*; Zeta Meter Corp.: New York, 1968.
- (39) Xu, R. *Particle Characterization: Light Scattering Methods*; Kluwer: New York, 2002.
- (40) Syngouna, V. I.; Chrysikopoulos, C. V. Transport of biocolloids in water saturated columns packed with sand: Effect of grain size and pore water velocity. *J. Contam. Hydrol.* **2011**, *126*, 301–314.
- (41) Hua, Z.; Tang, Z.; Bai, X.; Zhang, J.; Yu, L.; Cheng, H. Aggregation and resuspension of graphene oxide in simulated natural surface aquatic environments. *Environ. Pollut.* **2015**, *205*, 161–169.
- (42) Wu, L.; Liu, L.; Gao, B.; Munoz-Carpena, R.; Zhang, M.; Zhou, Z.; Wang, H. Aggregation kinetics of graphene oxides in aqueous solutions: Experiments, mechanisms, and modeling. *Langmuir* **2013**, *29*, 15174–15181.
- (43) Suresh, L.; Walz, J. Effect of surface roughness on the interaction energy between a colloidal sphere and a flat plate. *J. Colloid Interface Sci.* **1996**, *183*, 199–213.
- (44) Hoek, E. M. V.; Agarwal, G. K. Extended DLVO interactions between spherical particles and rough surfaces. *J. Colloid Interface Sci.* **2006**, *298*, 50–58.
- (45) Bradford, S. A.; Torkzaban, S. Colloid adhesive parameters for chemically heterogeneous porous media. *Langmuir* **2012**, *28*, 13643–13651.
- (46) Li, Y.; Wang, Y.; Pennell, K. D.; Abriola, L. M. Investigation of the transport and deposition of fullerene (C<sub>60</sub>) nanoparticles in quartz sands under varying flow conditions. *Environ. Sci. Technol.* **2008**, *42*, 7174–7180.
- (47) Johnson, W. P.; Pazmino, E.; Ma, H. Direct observations of colloid retention in granular media in the presence of energy barriers, and implications for inferred mechanisms from indirect observations. *Water Res.* **2010**, *44*, 1158–1169.
- (48) Anagnostopoulos, V. A.; Manariotis, I. D.; Karapanagioti, H. K.; Chrysikopoulos, C. V. Removal of mercury from aqueous solutions by malt spent rootlets. *Chem. Eng. J.* **2012**, *213*, 135–141.
- (49) Markou, G.; Mitrogiannis, D.; Çelekli, A.; Bozkurt, H.; Georgakakis, D.; Chrysikopoulos, C. V. Biosorption of Cu<sup>2+</sup> and Ni<sup>2+</sup> by *Arthrospira platensis* with different biochemical composition. *Chem. Eng. J.* **2015**, *259*, 806–813.
- (50) Freundlich, H. *Colloid and Capillary Chemistry*; Methuen and Co.: London, U.K., 1926.
- (51) Moore, R. S.; Taylor, D. H.; Sturman, L. S.; Reddy, M. M.; Fuhs, G. W. Poliovirus adsorption by 34 minerals and soils. *Appl. Environ. Microbiol.* **1981**, *42* (6), 963–975.
- (52) Anders, R.; Chrysikopoulos, C. V. Evaluation of the factors controlling the time-dependent inactivation rate coefficient of bacteriophage MS2 and PRD1. *Environ. Sci. Technol.* **2006**, *40* (10), 3237–3242.
- (53) Bellou, M. I.; Syngouna, V. I.; Tselepi, M. A.; Kokkinos, P.; Paparodopoulos, S. C.; Vantarakis, A.; Chrysikopoulos, C. V. Interaction of human adenoviruses and coliphages with kaolinite and bentonite. *Sci. Total Environ.* **2015**, *517*, 86–95.
- (54) Ho, Y.-S. Review of second-order models for adsorption systems. *J. Hazard. Mater.* **2006**, *136* (3), 681–689.
- (55) Azzizian, S. Kinetic models of sorption: a theoretical analysis. *J. Colloid Interface Sci.* **2004**, *276*, 47–52.

(56) Griffin, R. A.; Jurinak, J. J. Kinetics of the phosphate interaction with calcite. *Soil Sci. Soc. Am. Proc.* **1974**, *38*, 75–79.

(57) Upadhyayula, V. K. K.; Deng, S.; Smith, G. B.; Mitchell, M. C. Adsorption of *Bacillus subtilis* on single-walled carbon nanotube aggregates, activated carbon and NanoCeram. *Water Res.* **2009**, *43*, 148–156.

(58) Doherty, J.; Brebber, L.; Whyte, P. *PEST: Model-Independent Parameter Estimation*; Watermark Computing: Brisbane, Australia, 1994.

(59) Biggar, J. W.; Cheung, M. W. Adsorption of picloram (4-amino-3,5,6-trichloropicolinic acid) on panoche, ephrata, and palouse Soils: A thermodynamic approach to the adsorption mechanism. *Soil Sci. Soc. America J.* **1973**, *37* (6), 860–863.

(60) Khan, A. A.; Singh, R. P. Adsorption thermodynamics of carbofuran on Sn(IV) arsenosilicate in H<sup>+</sup>, Na<sup>+</sup> and Ca<sup>2+</sup> forms. *Colloids Surf.* **1987**, *24* (1), 33–42.

(61) Chowdhury, S.; Saha, P. D. Biosorption of methylene blue from aqueous solutions by a waste biomaterial: hen feathers. *Appl. Water Sci.* **2012**, *2* (3), 209–219.